

# Driven spin wave modes in XY ferromagnet: Nonequilibrium phase transition

*Muktish Acharyya*

*Department of Physics, Presidency University,  
86/1 College Street, Calcutta-700073, INDIA  
E-mail:muktish.physics@presiuniv.ac.in*

**Abstract:** The dynamical responses of XY ferromagnet driven by linearly polarised propagating and standing magnetic field wave have been studied by Monte Carlo simulation in three dimensions. In the case of propagating magnetic field wave (with specified amplitude, frequency and the wavelength), the low temperature dynamical mode is a propagating spin wave and the system becomes structureless or random in the high temperature. A dynamical symmetry breaking phase transition is observed at a finite (nonzero) temperature. This symmetry breaking is confirmed by studying the statistical distribution of the angle of the spin vector. The dynamic nonequilibrium transition temperature was found to decrease as the amplitude of the propagating magnetic field wave increases. A comprehensive phase boundary is drawn in the plane formed by temperature and amplitude of propagating field wave. The phase boundary was observed to shrink (in the low temperature side) for longer wavelength of the propagating magnetic wave. In the case of standing magnetic field wave, the low temperature excitation is a standing spin wave which becomes structureless (or random) in the high temperature. Here also, like the case of propagating magnetic wave, a dynamical symmetry breaking nonequilibrium phase transition was observed. A comprehensive phase boundary is drawn. Unlike the case of propagating magnetic wave, the phase boundary does not show any systematic variation with the wavelength of the standing magnetic field wave. In the limit of vanishingly small amplitude of the field, the phase boundaries approach the recent Monte Carlo estimate of equilibrium transition temperature.

**Keywords:** XY ferromagnet, Spin wave, Monte Carlo simulation, Propagating wave, Standing wave, Symmetry breaking, Dynamic phase transition

## I. Introduction:

The nonequilibrium responses of Ising ferromagnet to an oscillating (in time but uniform over the space) magnetic field is an interesting field of modern research[1, 2]. The the nonequilibrium phase transition is one major focus of investigation. Some important studies may be reported below. The existence of the growth of correlation near the transition was reported [3]. The bulk and surface critical behaviours was studied recently[4] and they belong to different universality class. The anomalous metamagnetic fluctuations near the transition was studied recently[5]. This study was supported by Monte Carlo simulation[6]. Experimentally, a notable transient behaviour was found[7], in the uniaxial cobalt film, for the faster than a critical time variation of the field. This is related to the the existence of first order transition. All these studies, mentioned above, is a signature of the current interest in the field of nonequilibrium responses of ferromagnets driven by time varying external magnetic field.

One important feature of the above mentioned studies are the time dependences of the external magnetic field which keeps the system away from equilibrium. However, recently the interests have been taken where the driving magnetic field has both spatio-temporal variation. This spatio-temporal variation has been incorporated as the propagating and standing magnetic field wave with specified amplitude, frequency and wavelength. The Ising ferromagnet driven by propagating magnetic field wave has been studied[8] by Monte Carlo simulation. The low temperature pinned (or frozen) phase was observed, where the spins are parallel and in a frozen state. Above a certain critical temperature the coherent propagation of spin bands is observed. The nonequilibrium dynamic transition is found and comprehensive phase boundary was obtained. In the case of standing magnetic wave [9], standing spin band modes (in the high temperature) are observed. The similar studies are performed with standing magnetic wave [10] in random field Ising ferromagnet and the exact mathematical form of the phase boundary is found, the breathing and spreading transitions are found in Ising ferromagnet driven by spherical magnetic wave [11], the dynamic transitions are studied in Blume-Capel model [12] driven by propagating and standing magnetic wave. The nonequilibrium multiple phase transition was observed[13] in Ising metamagnet driven by propagating magnetic field wave. All these studies mentioned above are perfomed in the discrete (Ising, Blume-Capel etc.) spin models.

The continuous ferromagnetic spin model like XY model has a very rich variety of behavious. The possibility of a very special kind of phase transition without long-range order was first proposed by Kosterlitz and Thouless [14] in planar magnets like two dimensional XY ferromagnets. After this remarkable discovery, the XY ferromagnet has drawn much attention of the researchers. The critical dynamics of two dimensional XY ferromagnet was studied[15] by Monte Carlo simulation. The surface critical behaviour was studied[16] in the XY model by Monte Carlo simulation. The Monte Carlo simulation was perfomed[17] in planar rotator model with symmetry breaking field. The vortex glass transition was found[18] in three dimensional XY model by Monte Carlo simulation. Recently, the quantum phase transition was found[19] in quantum XY model. The results of the critical properties of frustrated quasi two dimensional XY like antiferromagnet was reportet[20]. The magnetic properties of classical XY spin dimer in planar magnetic field was studied recently[21]. All the studies mentioned in this paragraph deal mainly with the *equilibrium* properties of XY model.

The *nonequilibrium* critical dynamics in XY model was also studied [22]. Nonequilibrium quantum phase transition using  $C^*$  algebra was studied recently [23]. Nonequilibrium phase transition in XY model with long range interaction was also studied [24]. The dynamical phase transition in

anisotropic XY ferromagnet driven by oscillating (in time but uniform over space) magnetic field was studied [25]. However, as far as the knowledge of this author is concerned, the nonequilibrium responses of XY ferromagnet to a magnetic field having both spatio-temporal variation, has not been studied so far.

In this paper, the nonequilibrium phase transition in XY ferromagnet, driven by propagating and standing magnetic field wave is studied by Monte Carlo simulation in three dimensions. The paper is organised as follows: Section-II describes the model and the Monte Carlo simulation method, the numerical results (with diagrams) are reported in section-III and the paper ends with a summary in section-IV.

## II. Model and simulation

The time dependent Hamiltonian of XY ferromagnet driven by a field having the spatio-temporal variation is expressed as

$$H(t) = -J \sum \cos(\theta(x, y, z) - \theta(x', y', z')) - \sum h(x, y, z, t) \cos(\theta(x, y, z)) \quad (1)$$

First term represents the interaction between spins at site x,y,z with its neighbouring (nearest) site x', y', z'. The x and y component of spin vector is represented by  $s_x$  and  $s_y$  respectively and  $s = \sqrt{s_x^2 + s_y^2} = 1$  here. The Spatio-temporal variations of the driving magnetic field have both (i) propagating wave form  $h(x, y, z, t) = H \cos[2\pi(ft - z/\lambda)]$  and (ii) standing wave form  $h(x, y, z, t) = H \sin(2\pi ft) \sin(2\pi z/\lambda)$ . The magnetic field wave propagates (or extends) along the z-direction and the field oscillates along the x-direction. The magnetic field wave is linearly (along x direction) polarised.  $J$  is the ferromagnetic ( $J > 0$ ) interaction strength. The magnitude of the field ( $h(x, y, z, t)$ ) is measured in the unit of  $J$ . A cubic lattice of size  $L$  ( $= 20$  here) is considered. It may be noted here that the dimensions of the system (lattice) are three (cubic) and the dimensions of the spin vector are two (XY model). The boundary conditions are taken as periodic in all three directions of the lattice.

The simulation starts from a random initial spin configuration corresponding to a very high temperature phase. At any finite temperature  $T$  (measured in the unit of  $J/k$ , where  $k$  is Boltzmann constant), a site (say x,y,z) is chosen randomly having an initial spin configuration (represented by an angle  $\theta_i(x, y, z)$ ). A new configuration of the spin (at site x,y,z) is also chosen (represented by  $\theta_f(x, y, z)$ ) randomly. The change in energy ( $\delta H(t)$ ) due to the change in configuration (angle) of spin (from  $\theta_i(x, y, z)$  to  $\theta_f(x, y, z)$ ) is calculated from equation (1). The probability of accepting the new configuration is calculated from the Metropolis formula[26]

$$P_f = \text{Min}[\exp(\frac{-\delta H(t)}{kT}), 1]. \quad (2)$$

An uniformly distributed random number ( $r = [0, 1]$ ) is chosen. The chosen site is assigned to the new spin configuration ( $\theta_f(x, y, z)$ ) if  $r \leq P_f$ . In this way,  $L^3$  number of sites are updated randomly.  $L^3$  number of such random updates defines a unit time step and is called Monte Carlo step per site (MCSS). The time in this simulation is measured in the unit of MCSS. Throughout the study the system size  $L$  ( $= 20$ ) and frequency  $f$  ( $= 0.01$ ) of the magnetic field wave are kept fixed. The total length of simulation is  $1.5 \times 10^5$  MCSS, out of which initial  $0.5 \times 10^5$  MCSS times are discarded. All statistical quantities are calculated over rest  $10^5$  MCSS.

The instantaneous components of magnetisations are  $Mx(t) = \frac{1}{L^3} \sum s_x(x, y, z)$   $= \frac{1}{L^3} \sum \cos(\theta(x, y, z))$  and  $My(t) = \frac{1}{L^3} \sum s_y(x, y, z) = \frac{1}{L^3} \sum \sin(\theta(x, y, z))$ . The time averaged magnetisations components over a full cycle (in time) of the magnetic field wave are defined as,  $Qx = f \oint Mx(t)dt$  and  $Qy = f \oint My(t)dt$ . Since the frequency  $f$  is taken equal to 0.01, 100 MCSS are required to have a complete cycle of the magnetic field wave. In  $10^5$  MCSS, 1000 such cycles are present. The  $Qx$  and  $Qy$  are calculated as the average over 1000 cycles. The variances of  $Qx$  and  $Qy$  are defined as  $Var(Qx) = L^3(\langle Qx^2 \rangle - \langle Qx \rangle^2)$  and  $Var(Qy) = L^3(\langle Qy^2 \rangle - \langle Qy \rangle^2)$ . The time averaged energy over the full cycles of the magnetic field wave is  $E = f \oint H(t)dt$  and the dynamic specific heat is defined as  $C = \frac{dE}{dT}$ .

### III. Results:

#### (a) Propagating wave:

The dynamical responses of the three dimensional XY ferromagnet driven by linearly polarised propagating magnetic field wave (described above) are studied. Starting from a random initial spin configuration the system is slowly (in the step  $\Delta T = 0.02$ ) cooled down to achieve a nonequilibrium steady state. Depending on the values of  $T$  and  $H$  two distinct dynamical phases are observed. In the low temperature, the coherent motion of bands of spins oriented along a particular directions (on average), is found. One such motion of spin bands are depicted in Fig. 1. The spin configuration of a XZ plane ( $Y=10$ ) is shown here. In the figure, the x-component of the spin lies along the horizontal axis and y-component of the spin lies on the vertical axis. Fig-1(a) and Fig-1(b) show the configurations (for  $T=0.4$  and  $H=3.0$ ) of spins at two different instants (1900 and 1930 MCSS) and the propagating modes of spin bands along the direction (upward) of propagation of magnetic wave is clear. This is propagating spin wave modes observed in XY ferromagnet driven by linearly polarised (along horizontal direction) magnetic wave. It may be noted here that magnetic wave propagates along the vertical direction and the y-component of spin is shown along the same direction. The lattice has dimensionality three (cubic system) whereas the spin has dimensionality two (XY model). This is the only way one can show the spin configuration of XZ plane in two dimensions. The low temperature spin configurations show that the x-component of spin is nearly zero, on an average. This is due to the response to the linearly (along x-direction) polarised propagating magnetic field wave. However, the y-component (on average) of the spin is nonzero. On the other hand, the high temperature ( $T = 2.6$ ) spin configuration (at instant  $t = 2000$ ) is completely random (or structureless) and has been shown in Fig-1(c). In this case, both x and y components of the spins are zero separately, on an average.

The propagating mode can also be visualised in the another way. The wave is propagating along the z direction. The y component of instantaneous planar magnetisation of any k-th XY plane is calculated as  $PMy(k) = \frac{1}{L^2} \sum s_y$ , where the sum is carried over all lattice sites of k-th XY plane. The planar magnetisation (y-component) is plotted against k for two different times and shown in Fig-2. From the figure the propagating mode is evident.

The dynamically stable spin structures in the low temperature of the system in response to the propagating magnetic field wave is also observed from the study of the statistical distribution of angles (of the spin). The angle  $\phi = \tan^{-1}(\frac{s_y}{s_x})$ , where  $s_x$  and  $s_y$  are the values of x and y component of the spin respectively. The distribution of  $\phi$  over all spins ( $L^3 = 8000$  here) are

calculated at any instant ( $t=2000$  here) for two different temperatures. One such distribution (unnormalised), for  $T = 0.3$  is shown in Fig-3(a). This distribution is trimodal. The three modes occur near  $\phi = 0$ ,  $\phi \simeq \pi$  and  $\phi \simeq 2\pi$ . The distribution vanishes at  $\phi = \frac{\pi}{2}$ . The distribution gets significantly valuable (nonzero) near  $\phi \simeq \frac{3\pi}{2}$ . This distribution of angle  $\phi$  assures the existence of a net y component with vanishingly small x component of spins. The high temperature ( $T = 2.6$ ) structureless spin configuration is justified by the distribution of angle ( $\phi$ ). This is shown in Fig-3(b), where the similar trimodal distribution is observed with almost equal weightage of angles  $\phi = 0, \pi$  and  $2\pi$  leading to vanish the net x component of spin. Similarly, almost equal weightage of angles  $\phi = \frac{\pi}{2}, \frac{3\pi}{2}$  compels net y component to vanish.

The components ( $M_x(t)$  and  $M_y(t)$ ) of instantaneous magnetisation are studied as functions of time and shown in Fig. 4. The x-component of instantaneous magnetisation  $M_x(t)$  is close to zero (apart from minor fluctuations) in the low temperature ( $T=0.4$ ). However, the y-component of this, shows a nonzero value (with some fluctuations). On the other hand, in the high temperature ( $T=2.6$ ) both vanish (fluctuate around zero). The system undergoes a *partial breaking of dynamical symmetry* ( $M_y(t)$  only) as it cooled down from high temperature. The low temperature partially dynamic symmetry broken phase is also evident from the distribution of angles discussed above.

From the usual definition of dynamic order parameter  $Q_x$  and  $Q_y$ , it is clear that as the system is cooled down,  $Q_y$  gets a nonzero value (corresponding to dynamically symmetry broken phase) from  $Q_y=0$  (corresponding to dynamically symmetric phase). It is needless to say that  $Q_x=0$  always. Fig. 5(a) shows the variation of  $Q_y$  as a function of temperature. There exists a critical temperature, below which  $Q_y \neq 0$ , is so called dynamic transition temperature. This dynamic transition temperature is found to decrease as the amplitude ( $H$ ) of the propagating field increases. The variance of  $Q_y$ , i.e.,  $\text{Var}(Q_y)$  is found to become sharply peaked at the transition point (Fig. 5(b)). From this diagram, the dynamic transition temperature, is determined and found to decrease as the amplitude of the field ( $H$ ) is increases. Interestingly, the dynamic transition point is also indicated by the maxima of the dynamic specific heat  $C$  studied as function of temperature  $T$  (Fig. 5(c)).

The dynamic transition temperatures are found to vary with wavelength of the propagating magnetic wave (for fixed value of amplitude). This is shown in Fig. 6. The dynamic order parameter  $Q_y$  and its variance  $\text{Var}(Q_y)$  are studied as functions of temperature ( $T$ ) for a two different values ( $\lambda = 20$  and  $5$ ) of wavelength of the propagating magnetic field wave (but with fixed amplitude  $H=2.0$ ). From the figure it is clear that, the system transits (order - disorder) at lower temperature (fixed  $H$ ) for longer waves of propagating magnetic field.

The dependences of the dynamic transition temperature, on the field amplitude and the wavelength of the propagating magnetic field wave, have been represented in a comprehensive manner in the phase diagram shown in Fig. 7. The phase boundaries are obtained for three different values of the wavelength ( $\lambda = 20, 10$  and  $5$ ) of the propagating magnetic wave. The phase boundary is found to shrink (towards low temperature and low field) inward for longer waves of the propagating field.

*(b) Standing wave:*

Now let us see what happens to the XY ferromagnet if it is driven by standing magnetic field wave. The standing magnetic field wave is extended along the z axis and the polarisation of the field is linear (along the x axis). Here also, two distinct dynamical modes are observed depending upon the values of  $T$  and  $H$ . For a fixed value of  $H = 3.0$  the low temperature ( $T = 0.4$ ) and high temperature ( $T = 2.6$ ) spin configurations of any XZ plane ( $Y=10$  here) are shown in Fig-8. In the

low temperature, the standing spin wave modes are observed and shown in Fig-8. Unlike the case of propagating spin wave modes, here the spin bands are formed but not changing their positions in time. Fig-8(a) and Fig-8(b) shows the spin configurations for two different instants ( $t = 1900$  and  $t = 1930$  MCSs). The spin bands are found not to change their positions in time. However, in the high temperature, the structureless or random spin configuration was observed (shown in Fig-8(c)).

The standing mode of driven spin wave in XY ferromagnet, can also be visualised in a different way. The  $y$  component of planar magnetisation  $PM_y(k)$  of  $k$ -th XY plane are plotted against  $k$  and shown in Fig-9 for two different times. From the diagram, it is clear that the profiles ( $PM_y(k)$  versus  $k$ ) do not change their relative positions in time (unlike the case of propagating mode shown in Fig-2).

The existence of the low temperature ordered (or structured) standing spin wave mode and the high temperature disordered (or structureless) dynamical states can be realised through the statistical distributions of the angles of the spins. The statistical distribution of the angle (of spin vector)  $\phi$  is studied and shown in Fig-10. The low temperature unnormalised distribution is shown in Fig-10(a). Here, the distribution is tetramodal (having four maxima). The angle  $\phi$  takes mostly four values: they are  $\phi = 0$ ,  $\phi \simeq \pi$ ,  $\phi \simeq 2\pi$  and  $\phi \simeq \frac{3\pi}{2}$ . It may be noted that, there was no peak in the distribution of  $\phi$ , near  $\frac{3\pi}{2}$ , in the case of propagating wave (compare with Fig-3(a)). The angle  $\phi$  dislikes to accept any value near  $\frac{\pi}{2}$ . This peculiar kind of distribution of angle  $\phi$  leads to net (nonzero)  $y$  component of magnetisation. The  $x$  component of magnetisation is zero on an average. This is characterised as dynamically ordered phase. On the other hand, the high temperature distribution of angle  $\phi$  (shown in Fig-10(b)) is almost symmetric and trimodal (having three maxima) around  $\phi = 0$ ,  $\phi \simeq \pi$  and  $\phi \simeq 2\pi$ . Needless to mention that this would lead to a vanishing net  $y$  component of magnetisation. The net  $x$  component of magnetisation is zero. This state is characterised as dynamically disordered phase. Like the case of propagating wave (already mentioned above), the ordered phase is a symmetry broken phase and the disordered one is symmetric (in all directions) phase. The partial (in  $y$  component only) symmetry broken is observed in the case of standing wave mode.

The dynamical symmetry breaking is clearly visible in the study of the time dependences of the components of magnetisation. The instantaneous components ( $M_x(t)$  and  $M_y(t)$ ) of magnetisation are studied as a function of time and shown in Fig-11. The high temperature ( $T = 2.6$ ) study (in Fig-11(a)) shows the existence of a dynamically symmetric phase where both  $M_x(t)$  and  $M_y(t)$  varies almost symmetrically around zero line. On the other hand, the low temperature ( $T = 0.4$ ) phase is a partially (through  $y$  component only) broken symmetric one (Fig-11(b)). In this case, only the  $y$  component  $M_y(t)$  varies asymmetrically (about zero line). So, a symmetry breaking dynamic (or nonequilibrium) transition is expected in the driven (by standing magnetic wave) XY ferromagnet. It may be noted that in both phases, the time average  $x$  component of magnetisation over the full cycle of the standing magnetic wave is zero.

To study the symmetry breaking dynamic phase transition in driven XY ferromagnet, the temperature dependences of  $Q_y$ ,  $Var(Q_y)$  and  $C$  are studied and shown in Fig-12. For a fixed value of  $H$ , the  $Q_y$  takes a nonzero value near a transition temperature as the system is cooled down from a high temperature. This transition temperature is found to decrease as the value of  $H$  is increased. This is shown in Fig-12(a). The  $Var(Q_y)$  and  $C$  show sharp peaks near the transition temperatures. They are shown in Fig-12(b) and Fig-12(c). The peaks determine the transition temperatures. From all these studies it is clear that the transitions occur at lower temperatures

for higher values of the field amplitudes ( $H$ ).

Obtaining the values of dynamic transition temperatures from the peak positions of  $Var(Q_y)$  and  $C$  for different values of the amplitudes ( $H$ ) the comprehensive phase diagrams are obtained and shown in Fig-13. Here also, the phase boundaries are drawn for three different ( $\lambda = 20, 10$  and  $5$ ) values of the wavelength of standing magnetic field wave. Unlike the case of propagating wave, the phase boundaries do not show any systematic variation with the wavelength of the standing magnetic wave, observed in this simulational study.

#### IV. Summary

The dynamical (or nonequilibrium) responses of classical XY ferromagnet driven by linearly polarised propagating and standing magnetic field wave have been investigated by Monte Carlo simulation using Metropolis algorithm in three dimensions. The system is a simple cube of length of each side  $L$  having periodic boundary condition in all three directions.

In the case of propagating magnetic field wave, with specified amplitude, frequency and the wavelength, the system shows various dynamical responses depending on the temperature. In the low temperature, the nonequilibrium steady state is dynamically structured. The coherent motion of the spin bands (or spin wave) was observed along the direction of the propagating magnetic field wave. In this phase, a nonzero net  $y$  component of magnetisation was observed with vanishing average  $x$  component. The  $y$  component varies asymmetrically (about zero) with time. The time averaged  $y$  component of the magnetisation over the full cycle of the propagating field wave (i.e., the  $y$  component of dynamic order parameter) is nonzero. On the other hand, the high temperature, dynamical state is structureless or randomly oriented. As a result both  $x$  and  $y$  components of the time averaged magnetisations, over the full cycle of the propagating magnetic wave, vanish. Both  $x$  and  $y$  component of the magnetisation varies symmetrically (about zero) with time. A partially (in  $y$  component only) symmetry breaking dynamic nonequilibrium phase transition was observed at any finite temperature. This symmetry breaking was observed independently from the distribution of the angles of the spin vectors. This transition temperature was found from the temperature dependences of dynamic order parameter, its variance and the dynamic specific heat. The dynamic transition was found to occur at lower temperature with higher values of the amplitude of the propagating field. A comprehensive nonequilibrium phase boundary was drawn in the plane formed by the temperature and amplitude of the propagating field wave. The phase boundary approaches the low temperature region for longer wavelength of the propagating magnetic field wave. A remarkable and interesting difference in the nonequilibrium phases, with that observed in the discrete spin models (Ising, Blume-Capel etc) [9, 12], is the absence of any pinned (or spin frozen) phase in the low temperature. The continuous spin models (like classical XY etc.) does not require any threshold field to change the state of individual spin which is essential for discrete spin systems. The phase boundaries were observed to approach the equilibrium critical temperature (around  $2.20J/k$ ) for vanishingly small field[29].

In the case of standing magnetic field wave, the low temperature nonequilibrium phase is a standing spin wave. Here also the symmetry breaking nonequilibrium phase transition was observed. The dynamic phase boundary was drawn. Unlike the case of propagating magnetic wave, here the phase boundary does not show any significant dependence on the wavelength of the standing magnetic field wave. However, like the case of propagating wave, the dynamic critical

temperature was observed to approach the equilibrium value [29] in the limit of vanishingly small field amplitude.

The dynamic phase transition is generally associated to the competition between the intrinsic time scale of the system (relaxation time) and the time scale (time period) of the external driving field (here, the propagating or standing wave). The reduction of dynamic transition temperature with the amplitude of the field is a result of the fact that the response time decreases with increasing the field amplitude.

This study is an appeal to the experimentalists to see the effect of spin dynamics in the ferromagnetic polycrystals like  $\text{Fe}[\text{Se}_2\text{CN}(\text{C}_2\text{H}_5)_2]_2\text{Cl}$  and  $\text{Zn}[\text{S}_2\text{CN}(\text{C}_2\text{H}_5)_2]_2$  which can be modelled by site diluted classical XY system [27] with superexchange interactions. In the field of spintronics [28] it is also important to know the response and thermodynamical behaviours of ferromagnetic systems driven by intense optical perturbations.

## References

1. B. K. Chakrabarti and M. Acharyya, Rev. Mod. Phys. **71** (1999) 847
2. M. Acharyya, Int. J. Mod. Phys. C, **16** (2005) 1631
3. R. Sides, P. A. Rikvold and M. A. Novotny, Phys. Rev. Lett. **81** (1998) 834
4. H. Park and M. Pleimling, Phys. Rev. Lett. **109** (2012) 175703; Erratum, Phys. Rev. Lett., **110** (2013) 239903
5. P. Reigo, P. Vavassori and A. Berger, Phys. Rev. Lett. **118** (2017) 117202
6. G. M. Buendia and P. A. Rikvold, Phys. Rev. E **96** (2017) 134306
7. A. Berger, O. Idigorus and P. Vavassori, Phys. Rev. Lett. **111** (2013) 190602
8. M. Acharyya, Physica Scripta, **84** (2011) 035009
9. A. Halder and M. Acharyya, J. Magn. Magn. Mater. **420** (2016) 290
10. M. Acharyya, J. Magn. Magn. Mater., **394** (2015) 410
11. M. Acharyya, J. Magn. Magn. Mater., bf 354 (2014) 349
12. M. Acharyya and A. Halder, J. Magn. Magn. Mater., **426** (2017) 53
13. M. Acharyya, J. Magn. Magn. Mater., **382** (2015) 206
14. J. M. Kosterlitz and D. J. Thouless, J. Phys. C: Cond. Mat. **6** (1973) 1181
15. E. G. Evertz and D. P. Landau, Phys. Rev. B **54** (1996) 12302
16. D. P. Landau, R. Pandey and K. Binder, Phys. Rev. B, **39** (1989) 12302
17. E. Rastelli, S. Regina and A. Tassi, Phys. Rev. B **69** (2004) 174407
18. P. Olsson, Phys. Rev. B **72** (2005) 144525
19. M. Guimaraes, B. V. Costa, A. S. T. Pires and A. Souza, J. Magn. Magn. Mater. **332** (2013) 103
20. R. S. Lapa and A. S. T. Pires, J. Magn. Magn. Mater., **327** (2013) 1
21. O. Ciftza and D. Prenga, J. Magn. Magn. Mater., **416** (2016) 220
22. L. Berthier, P. C. W. Holdsworth and M. Sellitto, J. Phys. A: Math. Gen. **34** (2001) 1805
23. S. Ajisaka, F. Barra and B. Zunkovic, New J. Phys. **16** (2014) 033028
24. T. N. Teles, F. Benetti, R. Parker and Y. Levin, Phys. Rev. Lett. **109** (2012) 230601
25. T. Yasui, H. Tutu, M. Yamamoto and H. Fujisaka, Phys. Rev. E, **66** (2002) 036123

26. N. Metropolis, A. W. Rosenbluth, M. N. Rosenbluth, A. H. Teller and E. Teller, *J. Chem. Phys.* **21** (1953) 1087
27. J. B. Santos-Filho and J. A. Plascak, *Phys. Lett. A*, **379** (2015) 3119
28. S. Bader and S. S. P. Parkin, *Ann. Rev. Cond. Mat. Phys.*, **1** (2010) 71-88
29. M. Hasenbusch, *J. Stat. Mech.* **12** (2008) P12006

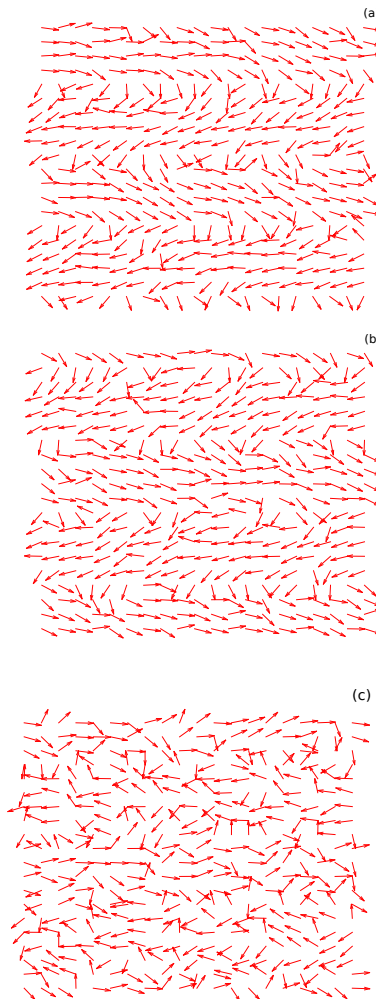


Figure 1: Coherent propagation of driven spin-wave in the XZ plane ( $Y=10$ ). Wave propagates along the vertical direction. (a)  $t = 1900$  MCSS and  $T = 0.4$ , (b)  $t = 1930$  MCSS and  $T = 0.4$  and (c)  $t = 2000$  MCSS and  $T = 2.6$ . Here, in all cases,  $L = 20$ ,  $f = 0.01$ ,  $\lambda = 10$  and  $H = 3.0$ .

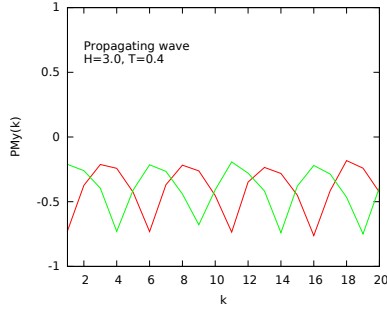


Figure 2: The y-component of planar magnetisation  $PM_y(k)$  plotted against  $k$  ( $k$ -th XY plane). Different colors represent different time (a)  $t=1900$  MCSS (red line) and (b)  $t=1930$  MCSS (green line). The propagating wave moves along  $z$  direction.

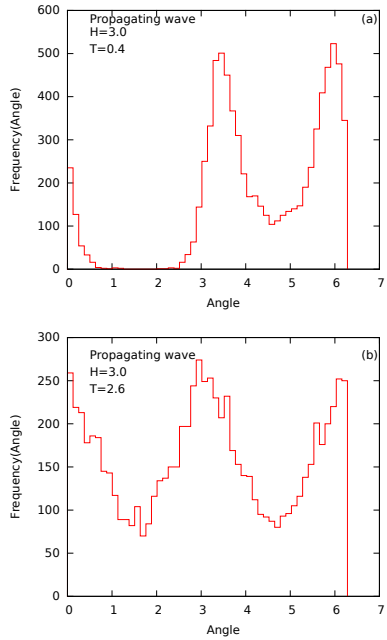


Figure 3: Unnormalized distribution of angles of the spin vectors for propagating waves. (a)  $t = 2000$  MCSS and  $T = 0.4$ , (b)  $t = 2000$  MCSS and  $T = 2.6$ . Here, in all cases,  $L = 20$ ,  $f = 0.01$ ,  $\lambda = 10$  and  $H = 3.0$ .

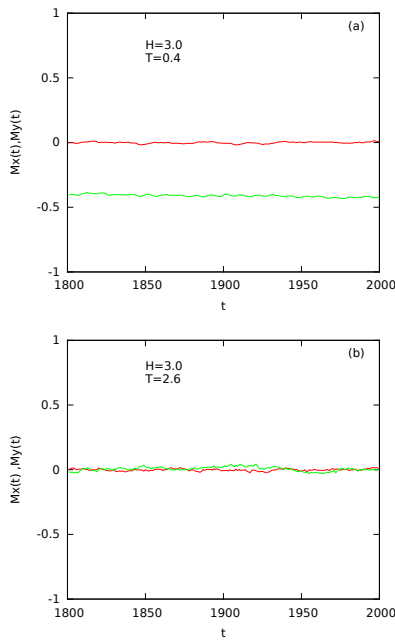


Figure 4: Breaking of the dynamical symmetry in the case of propagating wave. Plots of  $M_x(t)$  (red line) and  $M_y(t)$  (green line) as functions of time ( $t$ ) for different temperatures (a)  $T=0.4$  (symmetry broken phase) and (b)  $T=2.6$  (symmetric phase). In both cases,  $H=3.0$ ,  $f=0.01$  and  $\lambda = 10$ .

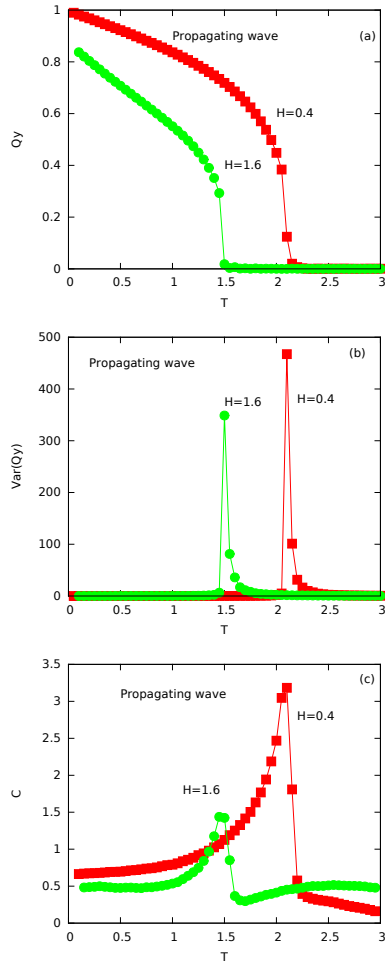


Figure 5:  $Q_y$ ,  $Var(Q_y)$  and  $C$  are plotted as functions of the temperature ( $T$ ) for two different values of the amplitude ( $H$ ) of propagating field wave. Here, in all cases,  $L = 20$ ,  $f = 0.01$ ,  $\lambda = 10$ .

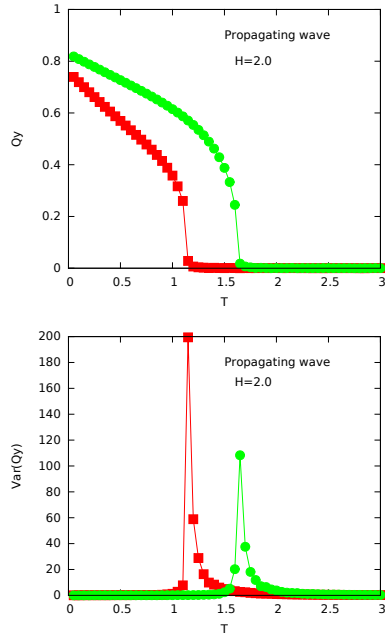


Figure 6:  $Q_y$  and  $\text{Var}(Q_y)$  are plotted as functions of the temperature ( $T$ ) for two different values of the wavelengths ( $\lambda$ ) of propagating field wave. Red square ( $\lambda = 20$ ) and Green bullet ( $\lambda = 5$ ). Here, in all cases,  $L = 20$ ,  $f = 0.01$  and  $H = 2.0$

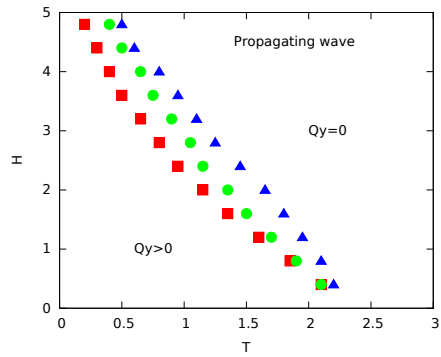


Figure 7: The phase diagrams for *propagating* wave. Different symbols correspond to the different values of wavelength ( $\lambda$ ). (Red square)  $\lambda = 20$ , (Green bullet)  $\lambda = 10$  and (Blue triangle)  $\lambda = 5$ .

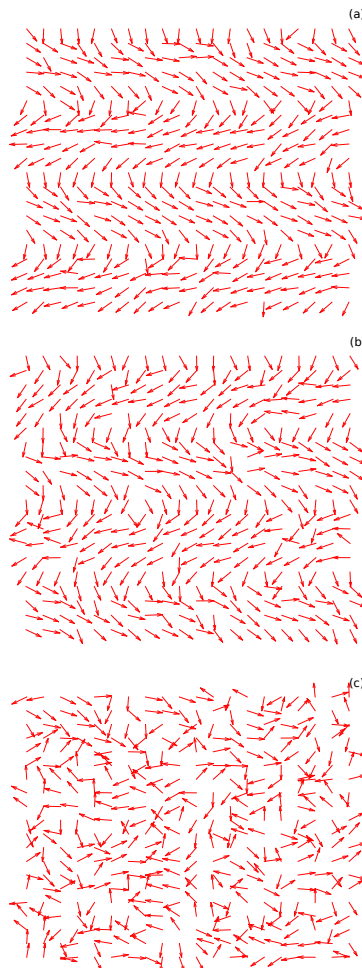


Figure 8: Standing mode of driven spin-wave in the XZ plane ( $Y=10$ ). (a)  $t = 1900$  MCSS and  $T = 0.4$ , (b)  $t = 1930$  MCSS and  $T = 0.4$  and (c)  $t = 2000$  MCSS and  $T = 2.6$ . Here, in all cases,  $L = 20$ ,  $f = 0.01$ ,  $\lambda = 10$  and  $H = 3.0$ .

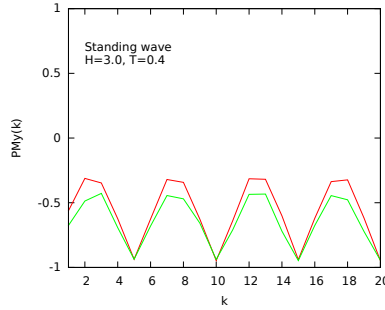


Figure 9: The y-component of planar magnetisation  $PM_y(k)$  plotted against  $k$  ( $k$ -th XY plane). Different colors represent different time (a)  $t=1900$  MCSS (red line) and (b)  $t=1930$  MCSS (green line). The standing wave extends along  $z$  direction.

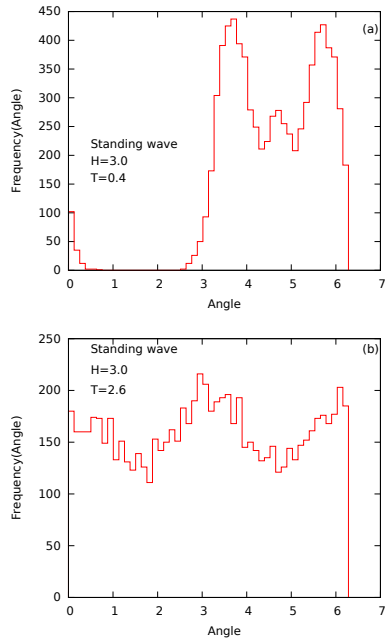


Figure 10: Unnormalized distribution of angles of the spin vectors for standing magnetic waves. (a)  $t = 2000$  MCSS and  $T = 0.4$ , (b)  $t = 2000$  MCSS and  $T = 2.6$ . Here, in all cases,  $L = 20$ ,  $f = 0.01$ ,  $\lambda = 10$  and  $H = 3.0$ .

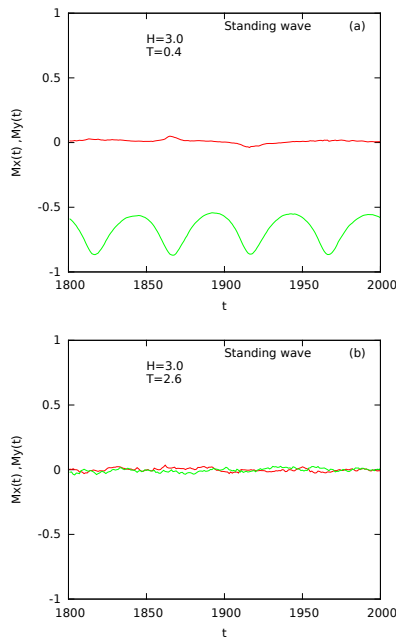


Figure 11: Breaking of the dynamical symmetry in the case of standing wave. Plots of  $M_x(t)$  (red line) and  $M_y(t)$  (green line) as functions of time ( $t$ ) for different temperatures (a)  $T=0.4$  (symmetry broken phase) and (b)  $T=2.6$  (symmetric phase). In both cases,  $H=3.0$ ,  $f=0.01$  and  $\lambda = 10$ .

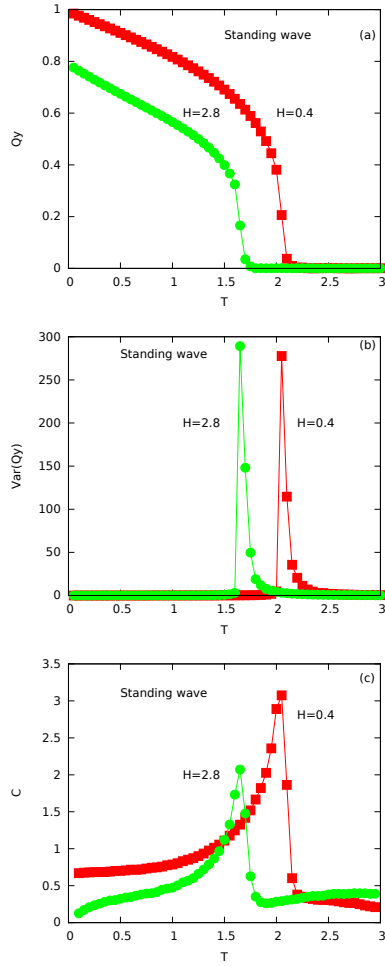


Figure 12:  $Q_y$ ,  $\text{Var}(Q_y)$  and  $C$  are plotted as functions of the temperature ( $T$ ) for two different values of the amplitude ( $H$ ) of standing magnetic field wave. Here, in all cases,  $L = 20$ ,  $f = 0.01$ ,  $\lambda = 10$ .

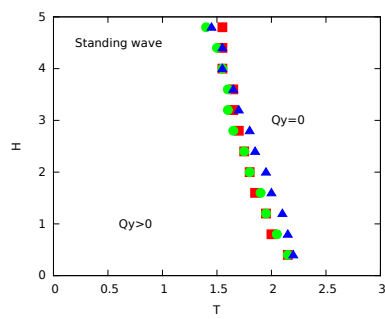


Figure 13: The phase diagrams for *standing wave*. Different symbols correspond to the different values of wavelength ( $\lambda$ ). (Red square)  $\lambda = 20$ , (Green bullet)  $\lambda = 10$  and (Blue triangle)  $\lambda = 5$ .